We are IntechOpen,
the world's leading publisher of
Open Access books
Built by scientists, for scientists

6,900
Open access books available

185,000
International authors and editors

200M
Downloads

154
Countries delivered to

Our authors are among the

TOP 1%
most cited scientists

12.2%
Contributors from top 500 universities

BOOK CITATION INDEX
CLARIVATE ANALYTICS
INDEXED

WEB OF SCIENCE™

Selection of our books indexed in the Book Citation Index
in Web of Science™ Core Collection (BKCI)

Interested in publishing with us?
Contact book.department@intechopen.com

Numbers displayed above are based on latest data collected.
For more information visit www.intechopen.com

Quality Control of the Microlenses Array

Rafał Kasztelanic
University of Warsaw
Poland

1. Introduction

Microlenses and microlens arrays, whose use in contemporary science and industry constantly increases, are objects which modify the phase of the light passing through those objects. Thus, in order to assess their characteristics and their quality one can measure either their shape, or the phase change they introduce.

Visualization and measurement of phase is an important element of various contemporary domains of science and industry. The first domain to use setups for measuring phase objects was biology. The possibility to observe almost transparent microorganisms or objects without the prior introduction of artificial coloring, has added to the development of biology and medicine. Another domain which has benefitted from measuring phase objects is astronomy. The needs of biologists on the one hand, and astronomers on the other, has forced the development of new technologies, methods of fabrication and measurement.

Yet another domain which benefits greatly from setups for measuring phase objects is the industry, including optical industry producing glasses and contact lenses. Changes in the setups for measuring phase objects have thus been induced by mass production for industrial purposes, miniaturization and by the need to add new characteristics and parameters. The methods which worked well for macroscopic objects did not bring satisfying results for microscopic ones. In the case of mass production dynamic quality control of phase objects and measuring the quality of large numbers of similar objects has become a must.

This chapter first focuses on describing various groups of methods used for measuring phase objects. Further on it presents the results of computer simulations and experimental realizations of an optical setup for automatic quality control of microlens arrays.

2. Methods used for measuring the phase

There are numerous methods which allow for the examination of phase objects. Generally such methods can be divided into four main groups: interferometric methods, methods based on focusing light, methods based on analyzing the direction of the light ray and methods based on modifying the spatial frequency of the phase object examined. The choice of the method depends on the precision of the measurement required, the specificity of the object to be measured and their cost-effectiveness.

2.1 Interferometric methods

Interferometric methods, used for transparent objects and objects reflecting light, do not directly measure the shape of the object or the phase change introduced by this object. The measurements are indirect: the methods allow for deducing the shape of the object on the basis of the distribution of the interferometric fringes and the distribution results from the phase change. A single light beam passes through or is reflected by the object examined, changing the phase of the light wave. This beam interferes with a reference beam to create a fringe pattern, where the fringes represent lines of constant phase. The location of the fringes bears information about the shape of the object examined.
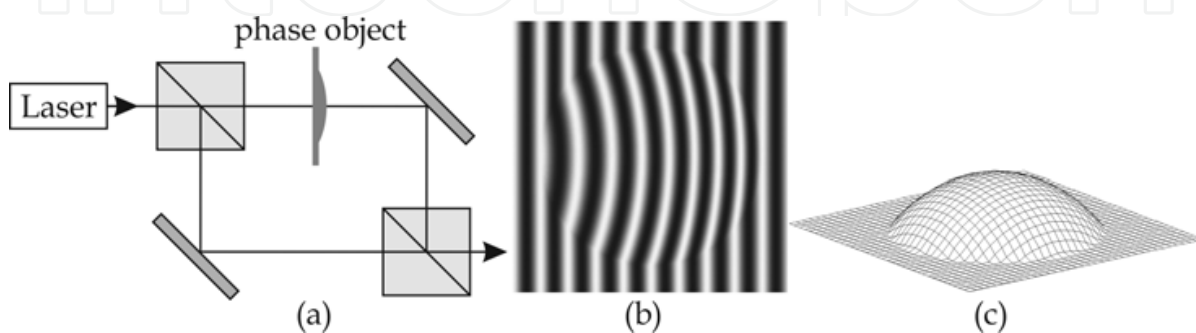

Fig. 1. An interferometric method. A scheme of the set-up a), an example of the interferogram b), shape reconstruction c)

The shape reconstruction of the object is carried out from the set of fringes with the use of relevant mathematical procedures, such as the Fourier transform, the windowed Fourier transform, the wavelet transform, the phase shifting or the phase stepping method, as well as frequency tracking methods etc.

For example, the phase stepping method uses three, four or five phase shifted fringe pattern images. In the case of four images it is possible to use a symmetrical phase shift by $\pi/2$:

$$\varphi = \left\{ -\frac{3}{4}\pi, -\frac{1}{4}\pi, \frac{1}{4} + \pi, +\frac{3}{4}\pi \right\} \tag{1}$$

In a two-beam interferometer, the corresponding phase-shifted intensity signals for a single image point in the fringe pattern are:

$$g_\varphi(\theta, v) = Q\left[1 + V\cos\left(\theta + v\phi_\varphi\right)\right] \tag{2}$$

where θ is the phase that we are interested in for surface profiling, V is the fringe visibility, $v \approx 1$ is the phase-shift frequency, with respect to the nominal or expected phase-shift sequence. The overall coefficient Q is the dc level of the signal. The algorithm which extracts the phase uses the following formula:

$$\theta = \arctan\left[\frac{-g_0 - g_1 + g_2 + g_3}{-g_0 + g_1 - g_2 + g_3}\right] \tag{3}$$

The main advantages of interferometric methods are their precision in the range of 0.1 nm, and the possibility of simultaneously measuring numerous parameters of the microlens, both optical and geometrical. The main disadvantage, however, is the size and the cost of

the setup. Apart from that, the precision of measuring small microlenses may often be problematic, as well as taking dynamic measurements in real time. Yet another problem when using the methods may be the presence of artifacts resulting from Fresnel diffraction, on the lens apertures, for instance.

Apart from all the above-mentioned problems, interferometric methods are most widely used because they are the most comprehensive.

2.2 Methods based on focusing light

Methods based on focusing light are direct methods which consist in measuring the shape of the surface. If the refraction index of the element examined is constant, it is possible to obtain information about the phase change.

The basis for the method is scanning the surface in order to measure the distance between the objective and the surface of the object. In each point of the object examined the setup is focused to obtain a sharp image, only one for each point. In this way information is gathered about each point of the object. As a result, information about its shape is reconstructed.

There are many types of focusing setups. One of the most widely used is the setup based on the confocal microscope.
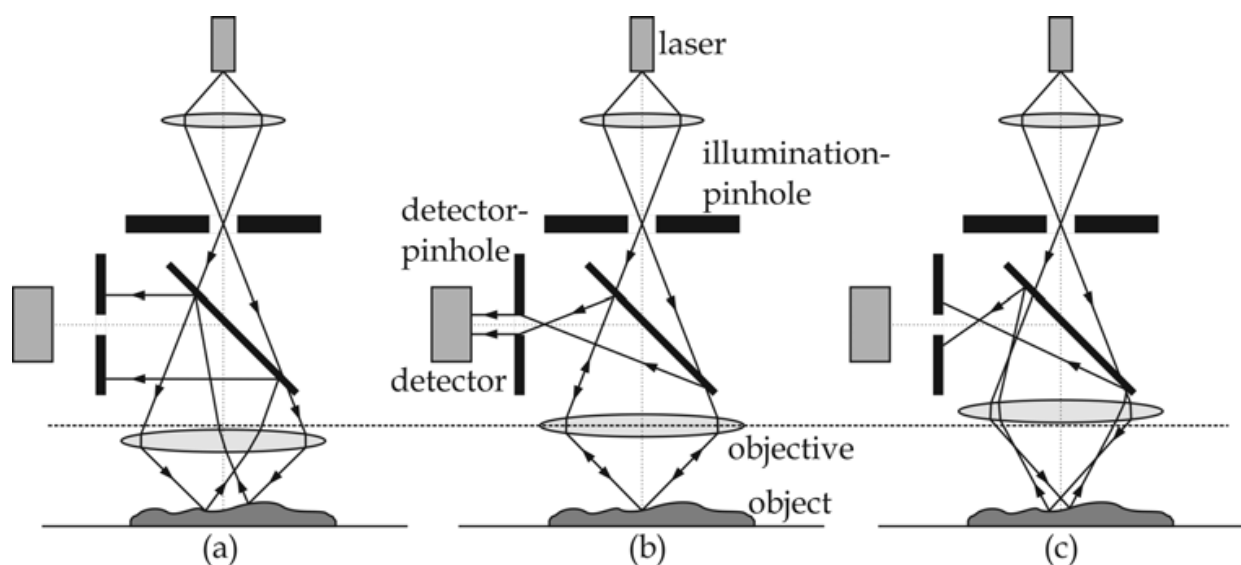

Fig. 2. Shape measuring with the use of confocal microscopy. Error in measuring the distance a) and c), the right measuring of the distance b)

The advantage of such setups is high precision of their vertical measurements, reaching 0.1 nm. Their horizontal resolution is lower, around 1 μm. The disadvantage is the time required for the measurement to take place, resulting from scanning the surface point by point, and the limitation in the size of the elements measured, also resulting from the scanning process. A strong point of the method is the possibility of using the stroboscopic light, which allows for measuring moving objects.

2.3 Methods based on analyzing the direction of the light ray

These indirect methods involve the analysis of the angles of the light rays leaving the phase object examined. The best known of these is the Shack-Hartmann filter based on microlens arrays. When illuminated by a plane wave, each of the microlenses focuses the light in its

own focal point. The non-uniformity in the location of the focal points reveals the distortions of the light wave. When the light beam is reflected, or passes through the object examined, its wave front changes. Its shape is now coded in the distribution of the bright points, the analysis of which allows for the reconstruction of the shape of the object examined.
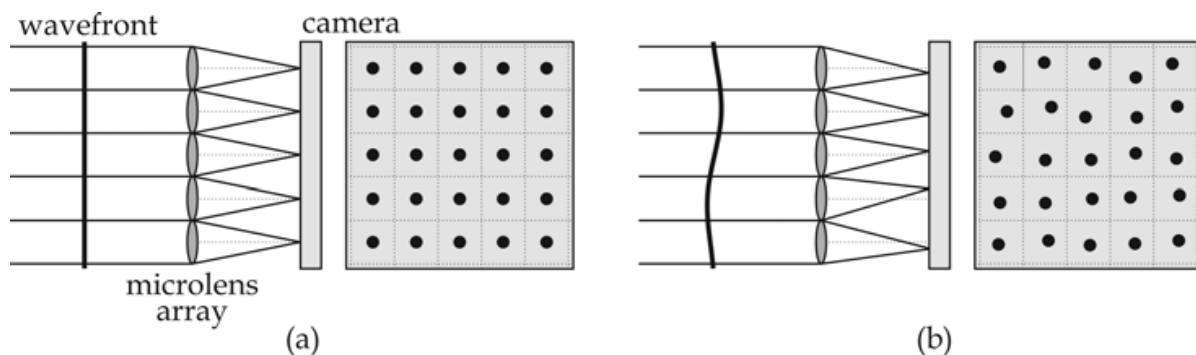

Fig. 3. Shack-Hartmann detector. Plane wavefront a), distorted wavefront b)

Such methods are predominantly used for examining the shape of the wavefront and find their uses, e.g. in astronomy and adaptive optical setups. Their main advantage is the short time of measurement. The main drawback is their relatively low horizontal resolution within the 30-50 μm range, as well as the fact that the results for large phase changes are difficult to interpret. That is why these methods are not used for measuring microlenses.

2.4 Methods based on modifying the spatial frequency

The last group comprises direct methods based on the modification of the light wave in the spatial frequency plane. Here, information about the phase of the object examined is based on the analysis of the intensity of light reflected or passing through the object, which is dependent on the real phase change. The method, where the light wave interferes with the light whose phase is shifted by ± π/2, comprises phase-contrast Zernike filters (Fig.4), as well as the schlieren, or knife edge method (also called a binary amplitude Foucault filter), and the Hilbert filter when realized as cutting or shifting a part of the spectrum of the object visualized. There is also the three steps Hoffman filter, where various fragments of the spectrum are blocked, or their intensity is diminished. The results obtained with these methods are primarily of qualitative character. The complex relation between the phase change of the input object and the light intensity on the output obtained in the measurement does not allow for the quantitative analysis, or limits such an analysis in a considerable way. That is why the use of these methods is highly limited. A possible solution is the use of spatial frequency filters where the intensity signal at the output of the setup carries information about the phase of the object examined, and is easy to interpret. The group includes the linearly graded filter (Settles, 2001), and the semiderivative filter (the square root filter) (Kasztelanic & Sagan, 2009).

3. Amplitude real filter

The use of the amplitude real filter to measure pure-phase objects is rooted in the methods for modifying spatial frequency. Its basis is a 4f correlator setup with a coherent light source. Its scheme is presented in Fig.5.

The phase object to be examined e.g. a microlens array is placed in the input plane of the correlator. The distorted wavefront is directed to the first lens (L1 - Fig.5). As a result, a distribution of the spatial frequencies of the examined field is obtained. This spectrum is filtered by the amplitude filter and the result of the transformation through the second lens (L2 - Fig.5) is an image in the output plane. The change of the light intensity in this image codes the information about the phase of the object examined. The exact form of the changes depends on the amplitude transmittance of the amplitude filters.
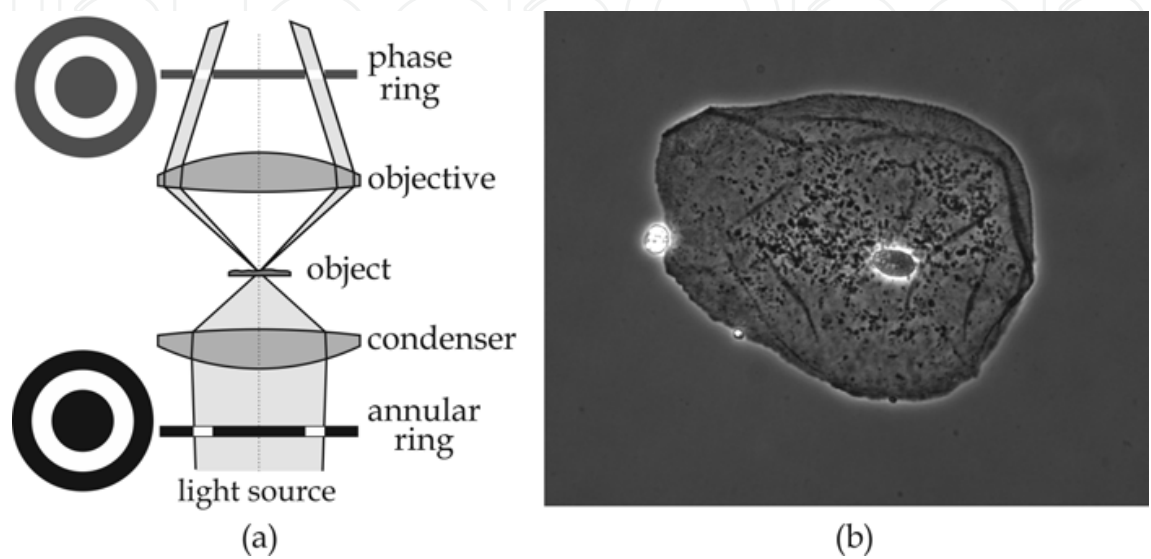

Fig. 4. Phase measuring with the use of phase-contrast Zernike filters a), sample result b)
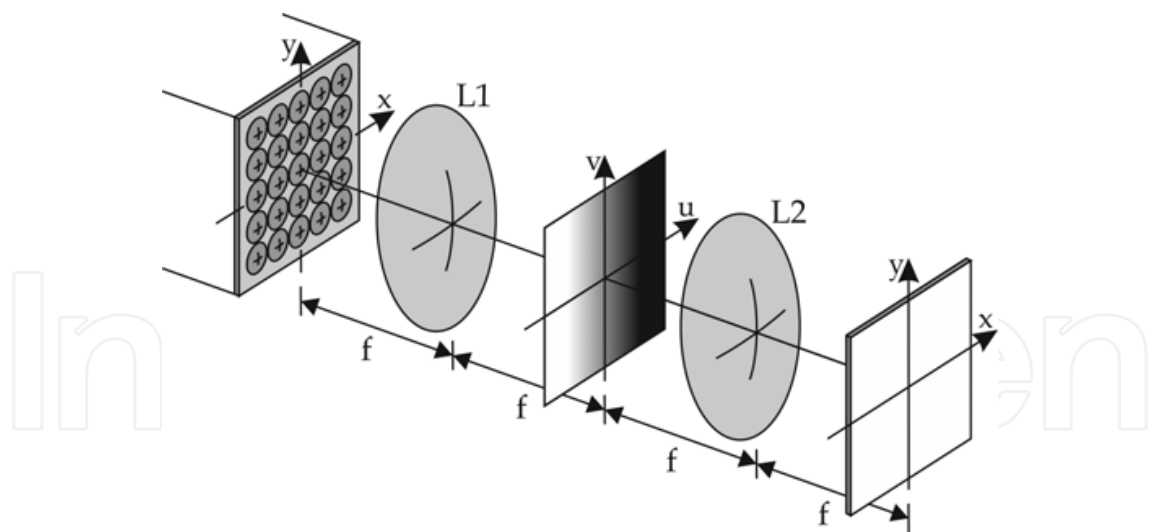

Fig. 5. The scheme of the setup for measurement of the quality of the microlens arrays

3.1 Linearly graded filter

Let us assume that the element examined is a pure-phase object and the object phase is described by the function $\theta(x,y)$. The transmittance of this object is equal to:

$$t(x,y) = \exp\left[i\theta(x,y)\right] \tag{4}$$

The amplitude transmittance of the linearly graded filter is defined as:

$$t(u,v) = \begin{cases} 0 & u < -\dfrac{w}{2} \\ a + \dfrac{u}{w} & -\dfrac{w}{2} \leq u \leq \dfrac{w}{2} \\ 1 & u > \dfrac{w}{2} \end{cases} \tag{5}$$

where a is the constant bias transmittance, typically equal to 0.5, and w is the spatial extent of the filter. Examples of amplitude transmittance profiles of this filter are presented in Fig.6.a). For a pure-phase object, it gives an output intensity distribution of:

$$I(x,y) = A_0^2 \left[a + \frac{\lambda f}{2\pi w} \frac{\partial \theta(x,y)}{\partial x} \right]^2 \tag{6}$$

where A_0^2 is the intensity of the illuminating beam, λ is wavelength of light and f is a focal length of lenses in the correlator.

3.2 Square root filter
The amplitude transmittance of the semiderivative real filter is defined as:

$$t(u,v) = \begin{cases} 0 & u < -\dfrac{w}{2} \\ \sqrt{a + \dfrac{u}{w}} & -\dfrac{w}{2} \leq u \leq \dfrac{w}{2} \\ 1 & u > \dfrac{w}{2} \end{cases} \tag{7}$$

where a, like in the previous equations, is the constant bias transmittance, typically equal to 0.5, and w is the spatial extent of the filter. Examples of amplitude transmittance profiles of this filter are presented in Fig.6.b). For a pure-phase object, it gives the output intensity distribution of:

$$I(x,y) = A_0^2 \left[a + \frac{\lambda f}{2\pi w} \frac{\partial \theta(x,y)}{\partial x} \right] \tag{8}$$

It is worth mentioning here that the result is not exact, while it is obtained through the rejection of the higher number of terms. However, as further shown, it does not influence the quality of the results in any considerable way.

The main advantage of using these filters lies in the fact that in the output the image of the light intensity is proportional to the first derivative of the gradient of the phase change in the object. The intensity is registered on the CCD camera and its distribution informs us about the shape of the object examined. The size of the observation area depends on the scale of the setup we use. The main disadvantage of the filter is the fact that the information about the gradient is one-directional only. In order to reconstruct the shape of the element examined, information about the gradient in two perpendicular directions is necessary. That is why all the measurements are carried out twice for each of

the filters: once with the filter set in the x direction and once in the direction perpendicular to the first one.
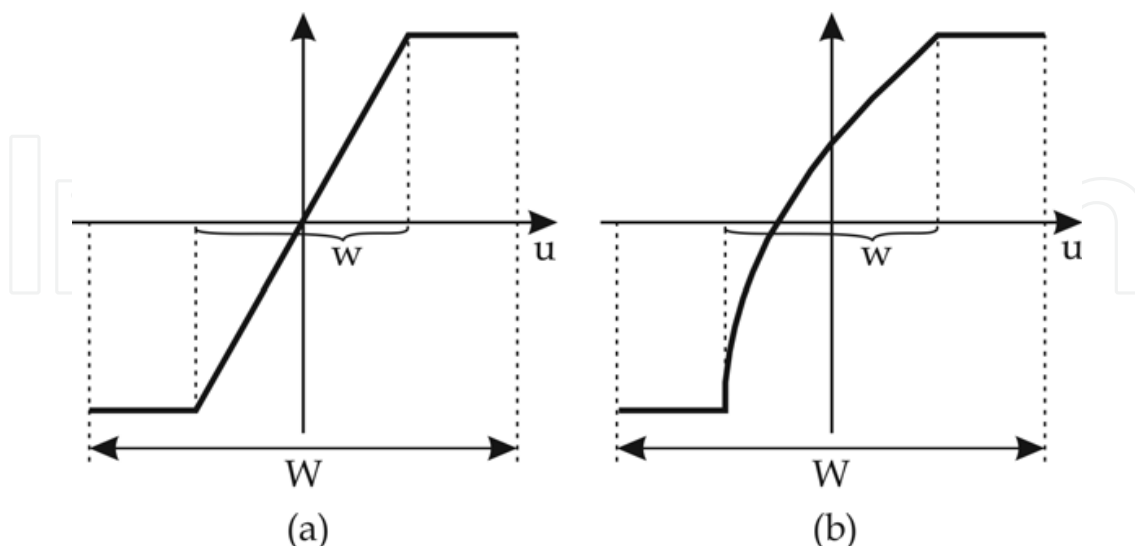

Fig. 6. The cross-section of the amplitude real filter: linearly graded filter a), square root filter (semiderivative) b). (W is the total width of the filter.)

4. Shape reconstruction with the use of the amplitude real filter

As a result of the work of the setup described above, an intensity signal is obtained. It codes the information about the phase gradient of the object examined. In order to reconstruct the real shape of the object on the basis of the data various techniques are used. Generally, the techniques use algorithms based on zonal estimation, modal estimation or a combination of both in a least-squares sense. These methods are used to analyze the wave front in the Shack-Hartmann detector. Of these, two methods will be presented at length. The Zernike polynomial expansion method gives more precise results but assesses the shape of the individual microlenses one by one when used for the analysis. The Fourier-based modal method allows for a simultaneous measurement of the shape of numerous elements. It is less precise but suitable for a fast analysis of the microelements' quality.

4.1 Zernike polynomials expansion method

In the case where the wave front distortion is introduced by such objects as a lens or a microlens arrays, in order to reconstruct the distortion, it is natural to use a method which gives information not only about the shape of the elements but also about the aberrations the shape introduces. One of such methods is the modal estimate method, which usually uses Zernike or Legendre polynomials, or complex exponentials as expansion functions. In the case of Zernike polynomials expansion method (Wyant & Creath, 1992), the shape of the wavefront W is given by the equation:

$$W(\rho,\theta) = \sum_m \sum_n C_n^m Z_n^m(\rho,\theta) \tag{9}$$

where C_n^m are the expansion coefficients, and Z_n^m are Zernike polynomials:

$$\begin{Bmatrix} Z_n^m(\rho,\theta) \\ Z_n^{-m}(\rho,\theta) \end{Bmatrix} = R_n^m(\rho) \begin{Bmatrix} \sin(m\theta) \\ \cos(m\theta) \end{Bmatrix} \tag{10}$$

and where R_n^m is the radial coefficient equal:

$$R_n^m(\rho) = \sum_{k=0}^{(n-m)/2} \frac{(-1)^k (n-k)!}{k! \left[\dfrac{n+m}{2}-k\right]! \left[\dfrac{n-m}{2}-k\right]!} \rho^{n-2k} \quad n=0,1,2,... \ \ (n-m)\text{even} \tag{11}$$

Such a description opens up the possibility of an easy comparison of the shape of the lens examined with the ideal lens. An additional advantage here is the fact that some polynomials of Zernike series have recognizable optical properties. For instance, the polynomial Z_2^0 describes the optical property of 'defocus', the polynomial Z_4^0 describes the 'spherical aberration' and the polynomials Z_2^{-2} and Z_2^2 describe the 'astigmatism'. In the case of a microlens arrays polynomial expansion opens an additional possibility of comparisons between the particular lenses.

Further on, single indexation of Zernike polynomials with the j parameter is used, due to the fact that it is easier to use and present the results. The j parameter is calculated on the basis of m and n parameters as j=[n(n+2)+m]/2.

The reconstruction of the shape of the optical element examined is carried out on the basis of the information about the phase gradient change measured in two perpendicular directions and is possible after differentiation of Eq. 9:

$$\frac{\partial \theta}{\partial x} = \sum_{k=0}^{M} a_k \frac{\partial Z_k(x,y)}{\partial x}, \quad \frac{\partial \theta}{\partial y} = \sum_{k=0}^{M} a_k \frac{\partial Z_k(x,y)}{\partial y} \tag{12}$$

where $Z_k(x,y)$ are the kth Zernike polynomials and M is the number expansion of coefficients a_k. In the matrix form it could be written as:

$$S = Aa \tag{13}$$

where A is a gradient rectangular matrix and M the number of columns. The number of rows is equal to the sum of pixels in the two images of the gradient along the x and y axes. The solution of Eq. 13 can be found on the basis of equation:

$$a = \left(A^T A\right)^{-1} A^T S. \tag{14}$$

4.2 Fourier-based modal method

In the case when the wavefront distortion is introduced by numerous objects such as microlenses, it is more convenient to reconstruct the shape of the distortion for all the objects simultaneously. An example of such an approach is the Fourier-based modal method (Guang-ming Dai, 2008).

Assuming that A is the shape of the wavefront, and a is the spectrum of this front, it is easy to note a relation between the two:

$$A(x,y) = F^{-1}\{a(u,v)\} = \iint a(u,v)\exp[2\pi i(xu+yv)]\,du\,dv \tag{15}$$

$$a(u,v) = F^{-1}\{A(x,y)\} = \iint A(x,y)\exp[-2\pi i(xu+yv)]\,du\,dv \tag{16}$$

where F{ }, F⁻¹{ } mean the Fourier transform and the inverse Fourier transform, respectively. In the correlator setup with a linear or square root filter, the output image is proportional to the gradient of the phase change. Using such two setups with mutually perpendicular filters we obtain two signals:

$$\begin{cases} \dfrac{\partial A(x,y)}{\partial x} = 2\pi i \iint u\, a(u,v)\exp[2\pi i(xu+yv)]\,du\,dv \\[2mm] \dfrac{\partial A(x,y)}{\partial y} = 2\pi i \iint v\, a(u,v)\exp[2\pi i(xu+yv)]\,du\,dv \end{cases} \tag{17}$$

Introducing the notifications:

$$b_x(u,v) = 2\pi i\, u\, a(u,v) \tag{18}$$

$$b_y(u,v) = 2\pi i\, v\, a(u,v) \tag{19}$$

and consequently multiplying by u on both sides of Eq.18 and v on both sides of Eq.19 combining them yields:

$$u\, b_x(u,v) + v\, b_y(u,v) = 2\pi i\,(u^2+v^2)\, a(u,v) \tag{20}$$

to finally obtain the spectrum of the wevefront examined:

$$a(u,v) = -i\,\frac{u\, b_x(u,v) + v\, b_y(u,v)}{2\pi(u^2+v^2)} \tag{21}$$

The final shape of the wavefront distortion is obtained after the inverse Fourier transform:

$$A(x,y) = F^{-1}\left\{-i\,\frac{u\, b_x(u,v) + v\, b_y(u,v)}{2\pi(u^2+v^2)}\right\} = F^{-1}\left\{-i\,\frac{u F\left\{\dfrac{\partial A(x,y)}{\partial x}\right\} + v F\left\{\dfrac{\partial A(x,y)}{\partial y}\right\}}{2\pi(u^2+v^2)}\right\}. \tag{22}$$

5. Computer simulation

Computer simulations were carried out in order to examine the work of the setup presented in Fig.5 and to establish how the kind of the amplitude filter and its parameters influence the results obtained.

As test objects various lenses were used, whose shape can be given by the equation:

$$h(r) = \frac{h_0}{R}\frac{r^2}{1 + \sqrt{1 - (K+1)r^2/R^2}} \tag{23}$$

where h(r) is the height of the lens as a function of the distance r to the optical axis, R is the radius of curvature at the vertex, h_0 is the maximum height and K is the aspherical constant. The lens profile h(r) might be spherical (K=0), elliptic (1<K<0 or K>0), parabolic (K=-1) and hyperbolic (K<-1). In the simulations it was assumed that K=-1.5 for hyperbolical lenses and K=-0.5 for elliptical lenses.

The parameters of the optical setup used for the simulations were the following: the wavelength of λ=632.8 nm, the focus L1 and L2 of the setup from Fig.5 f=100 mm, the lens diameter D≈8.2 mm, the size of a single pixel 1μm. The propagation method used was Rayleigh-Sommerfeld propagation.

In the first steps of the simulation the pure phase element to be examined was a single microlens, 100 μm in diameter, placed in the optical axis of the setup. The first simulations checked the influence of the spatial extent of the filter w on the quality of the lens reconstruction. In order not to block high spatial frequency the spatial extent should be as large as possible. However, in accordance with Eq.6 and Eq.8 it cannot be too large because this parameter influences the range of modulation of the light intensity in the output of the setup. In the simulation it was assumed that the maximum size of the filter W is calculated on the basis of the maximal gradient of the examined lenses. The change of the light phase of the λ wavelength, in the lens with refraction index n, and shape given by Eq.23 can be defined as:

$$\theta(r) = h(r)\frac{2\pi(n-1)}{\lambda} \tag{24}$$

The maximal gradient can be found on the edge of the lens, for r=R/2, and thus we obtain:

$$\left.\frac{\partial\theta(r)}{\partial r}\right|_{\substack{max \\ r=R/2}} = \frac{h_0\,2\pi(n-1)}{\lambda\,\sqrt{3-k}} \tag{25}$$

Calculating further the spatial frequency and passing on to the object domain after the transform by the lens of focal length f we obtain the maximum size of the filter:

$$W = 2f\,h_0(n-1)\big/\sqrt{3-k} \tag{26}$$

As the measurement of the error made when reconstructing the element examined it was assumed that:

$$E = \sum_S (H_S - h_S)^2 \tag{27}$$

where the sum comprises the whole the whole area of the lens S, while H_S and h_S are the height of the original and the measured lens, respectively.

As the measurement of the error made when reconstructing the element examined with Zernike expansion it was assumed that:

$$\sigma^2 = \sum_{k=0}^{M} \left(a_k - c_k \right)^2 \qquad (28)$$

where c_k are Zernike coefficients of the lens examined and a_k are Zernike coefficients calculated on the basis of the images obtained for linear graded and semiderivative filters of various width.

Fig. 7 presents the simulation of the change in the quality of reconstruction with the use of Fourier modal method. The reconstruction is carried out for the test lenses and for two kinds of filters: the semiderivative and linearly graded filter, with regards to the filter width w and the camera of 8 Bit dynamic range.

The results show that there is an optimal width of the filter w, for which minimal errors are obtained. For both the filters the optimum width is within the range of 0.1 and 0.2 of the maximum filter with, given by Eq.26, independently from the shape of the lens examined. If the filter is too wide, it gives bigger errors due to the low modulation of the signal obtained. Changing the dynamic range of the camera over 10 Bit improves the results if the filter size is not precisely adjusted, however, it does not influence the minimal reconstruction error in a considerable way (Fig.8.a). A very narrow filter generates big errors because then it acts similarly to the knife edge filter. As a result of the work of such a filter, the intensity obtained in the output, which carries information about the phase change, has a more complicated form than the simple proportion to the gradient of the phase changes.
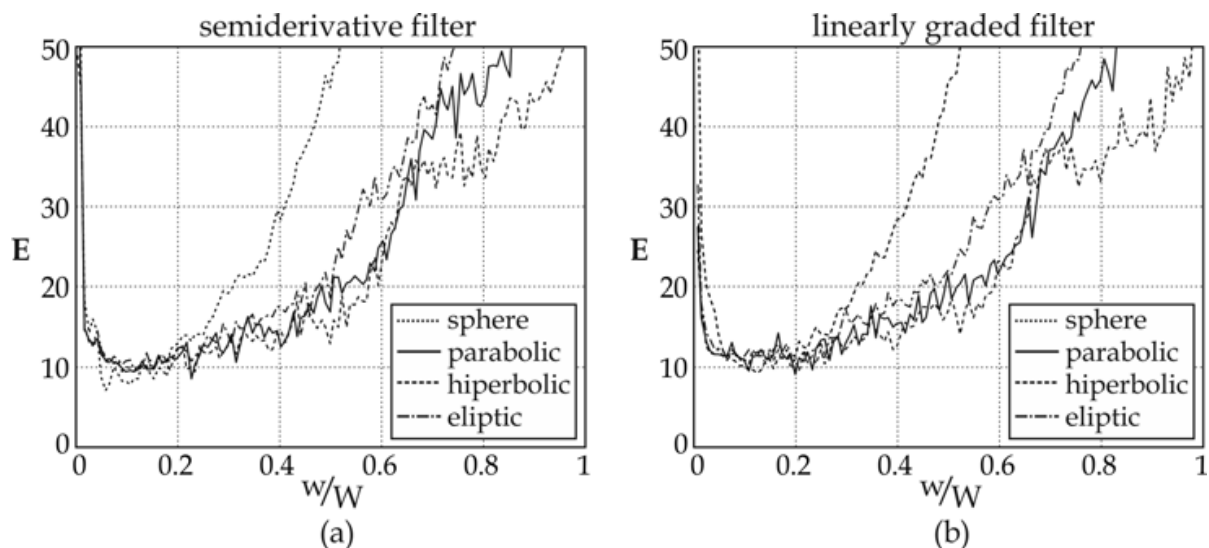

Fig. 7. E error in the reconstruction of the shape of the lenses carried out with the use of the Fourier modal method, depending on the kind of filter and its width: semiderivative filter a), linearly graded filter b)

The occurring reconstruction errors (Fig.8b) reach 1% of the total thickness of the microlens (100% error is obtained for flat surfaces). However, the size of the error depends only on the slight degree on the number of the microlenses simultaneously undergoing reconstruction (Fig.9). Thus, the Fourier-based modal method will not be successful where it is important to precisely establish the shape of the lens. On the other hand, the reconstruction errors are small enough to be disregarded when the method is used for a fast quality control. Thus, the

method allows for a fast assessment of the lenses' shape, which in turn, allows for depicting errors in microlens arrays at the fabrication stage.
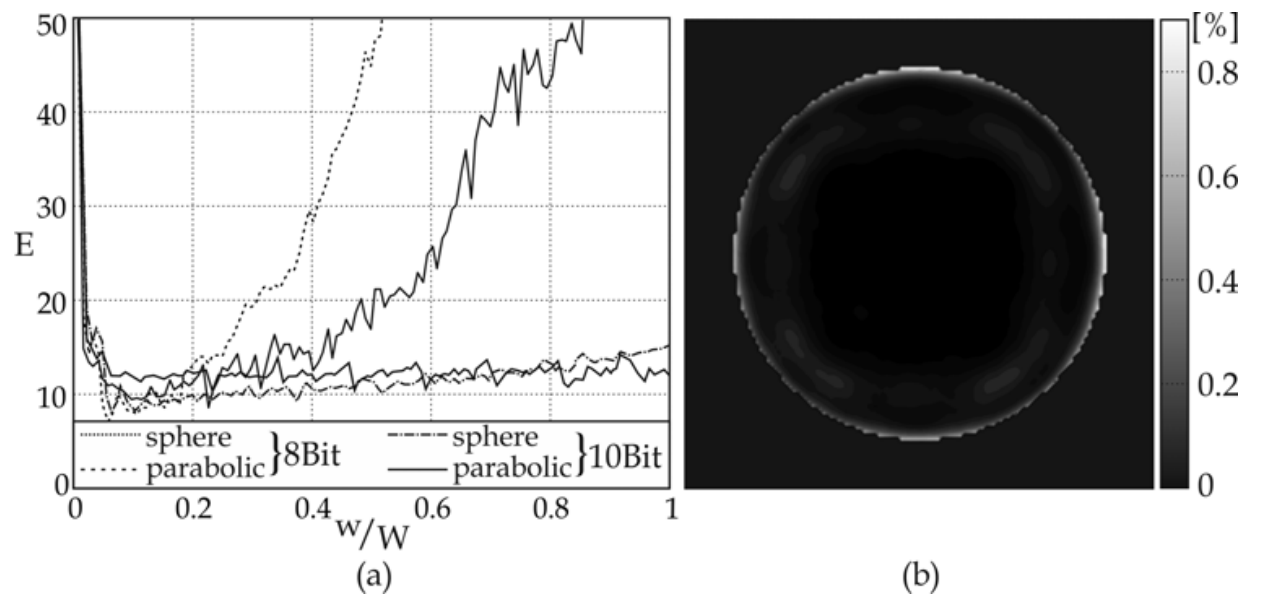

Fig. 8. Error E in the reconstruction of the lens shape with the use of the Fourier modal method for the camera with 8 and 10 Bit dynamic range a) and the image of the reconstruction error of the spherical lens reconstructed with the use of the semiderivative filter for a camera with an 8 Bit dynamic range b)
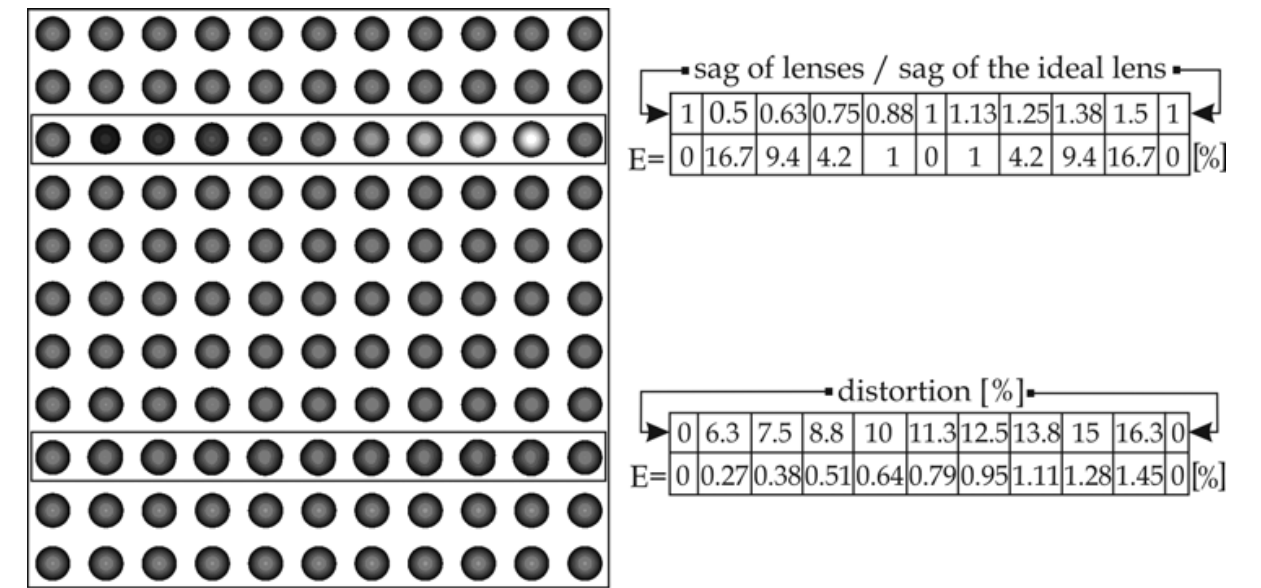

Fig. 9. The results of the reconstruction of the shape of a microlenses array with the use of Fourier modal method a) error E of the shape reconstruction for two modified rows of microlenses b)

Fig.9 presents the reconstruction of an 11x11 array of microlenses, 75 µm in diameter and lying within the distance of 100 µm. Apart from the two marked rows, all the remaining lenses have the same shape. The lenses marked in the upper row have a different height,

and vary from 0.5 to 1.5 as compared to the height of the original lens. The lenses in the lower row have shapes different from the original. Their shape has been distorted by adding 36 consecutive Zernike polynomials, which has resulted in the shape changes between 6.25% and 16.25% of the original lens shape.

The results obtained show that all the lenses with the regular shape have been correctly reconstructed, and the reconstruction error is close to zero. On the other hand, while reconstructed, the distorted lenses differ from the original ones. The reconstruction error, as compared to the original shape, allows for the assessment of the size of the distortion.

In the case of the reconstruction using the Zernike polynomials expansion method, the reconstruction errors are smaller. Fig.10 presents the simulation of the change in the quality of the reconstruction of the test parabolic lens with an added distortion, with regards to the filter width w and for the camera of 8 and 10 Bit dynamic range. The results show that there is an optimal width of the filter w, for which minimal errors are obtained, both for the shape reconstruction and Zernike polynomial expansion. The width depends on the type of the amplitude filter used.
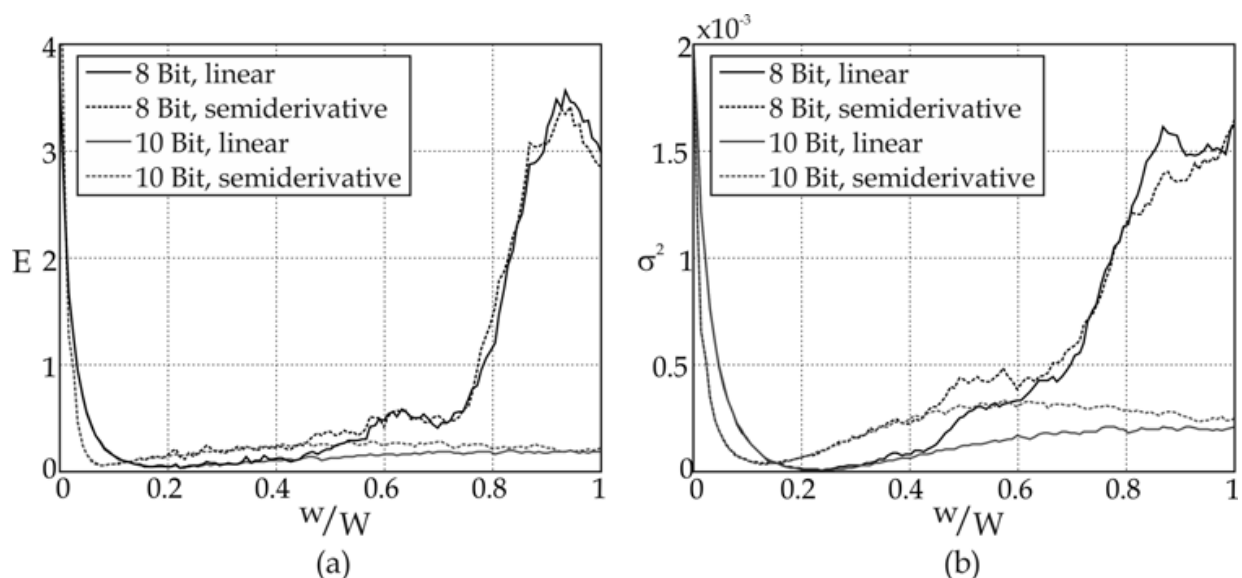

Fig. 10. E error in the reconstruction of the shape of the parabolic lens with the use of the Zernike polynomials expansion method a) and σ^2 error of Zernike polynomial expansion b) with regard to the kind of filter for the camera with 8 and 10 Bit dynamic range

Another series of simulations helped to estimate how the basic shape of the microlens examined influences the quality of the reconstruction and whether it is possible to recognize such a shape. In the simulations expansion for 36 Zernike polynomial and 10 Bit dynamic range of the camera have been assumed. Fig.11.a) presents the results for a linear filter. The results for the semiderivative filter are similar, but the error is bigger. In the case of spherical lenses the error is increased by 1.5 factor, and the results for the remaining lenses decrease by about an order of magnitude. From the simulation it is also possible to infer the shape of the lens examined, by choosing the characteristic elements of the 0, 4th and 12th terms. Especially, it is the 12th element of Zernike expansion which allows for establishing this shape. On the other hand, having the data about the original shape of the lens, it is possible, to obtain information only about the deviations of the real shape from the ideal one.
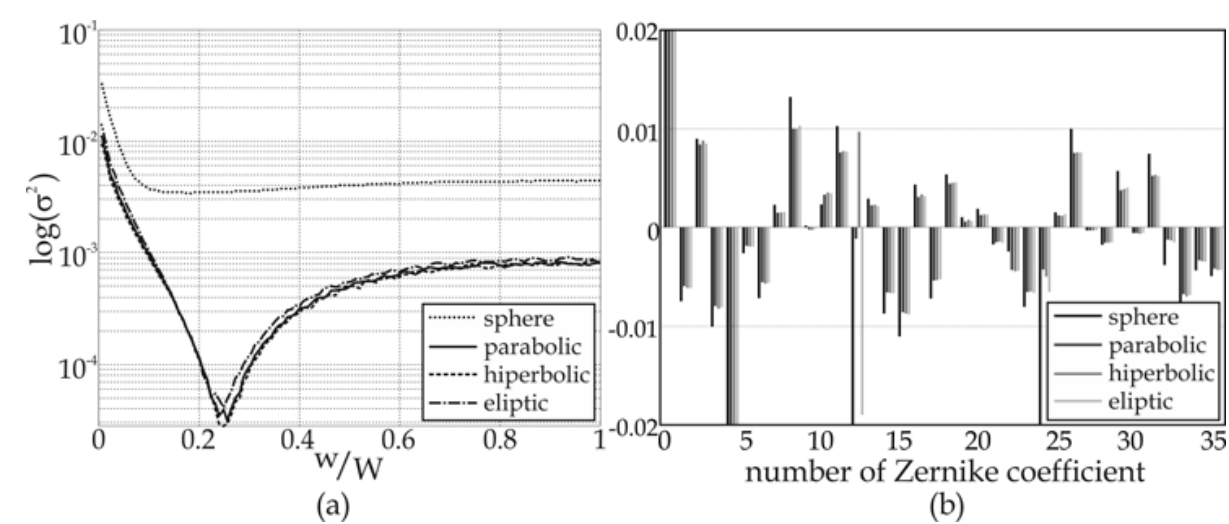
Fig. 11. The results of the reconstruction of variously shaped lenses by the linear filter with the use of the Zernike polynomials expansion method. The error made during the reconstruction a), values of Zernike expansion coefficients b)

It has also been checked how the preciseness of reconstruction changes depending on the location of the lens, with regards to the optical axis and on the size of the microlens arrays. The simulations carried out for the 15x15 array of lenslet pitch equal 250 µm show that there are slight differences in the reconstruction depending on the place of the location. In the case of σ^2 , the spread of the results is within 1% for all the lens types and for both filters used.

6. Experimental realization of the 4f correlator

The experimental realization of the 4f correlator based on lenses with the focus of 100 mm and the diameter of 51.2 mm, as well as a CCD camera with 14 Bit dynamic range. A low-cost method based on commercial slide imagers was used to fabricate grayscale amplitude filters. The smallest feature of the filter obtained in this way was about ~4.5 µm (Fig.12).
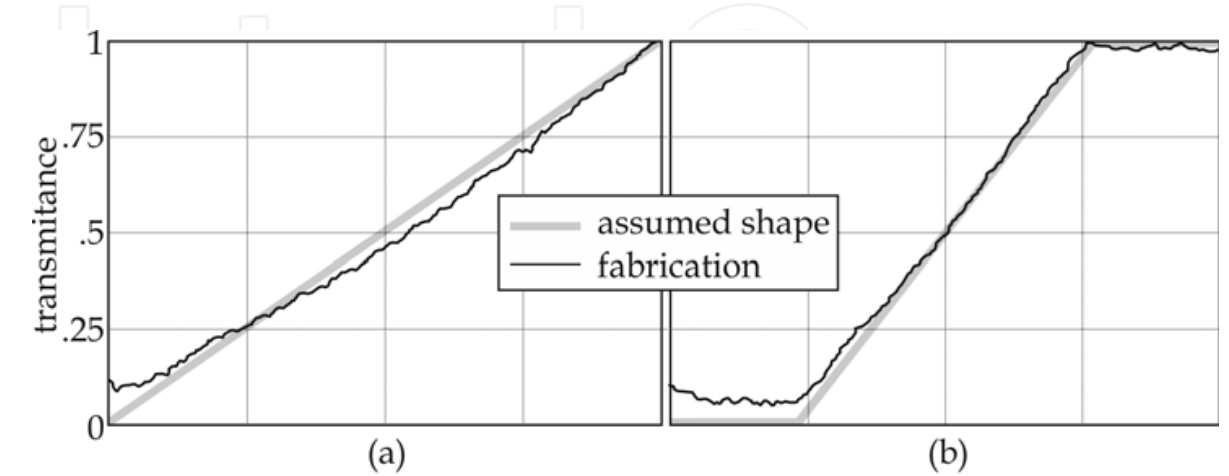

Fig. 12. Intensity transmittance of the fabricated square root filter before optimization a) and after optimization b)

The first experiments examined the quality of reconstruction of the microlens arrays. The experiment used a commercially available array of plano-convex microlenses arranged in a square grid of 146 μm in diameter, 150 μm lenslet pitch and 6.7 mm focal length produced by ThorLabs. Two images of microlenses were registered with the two mutually perpendicular locations of the amplitude filter (Fig.13).
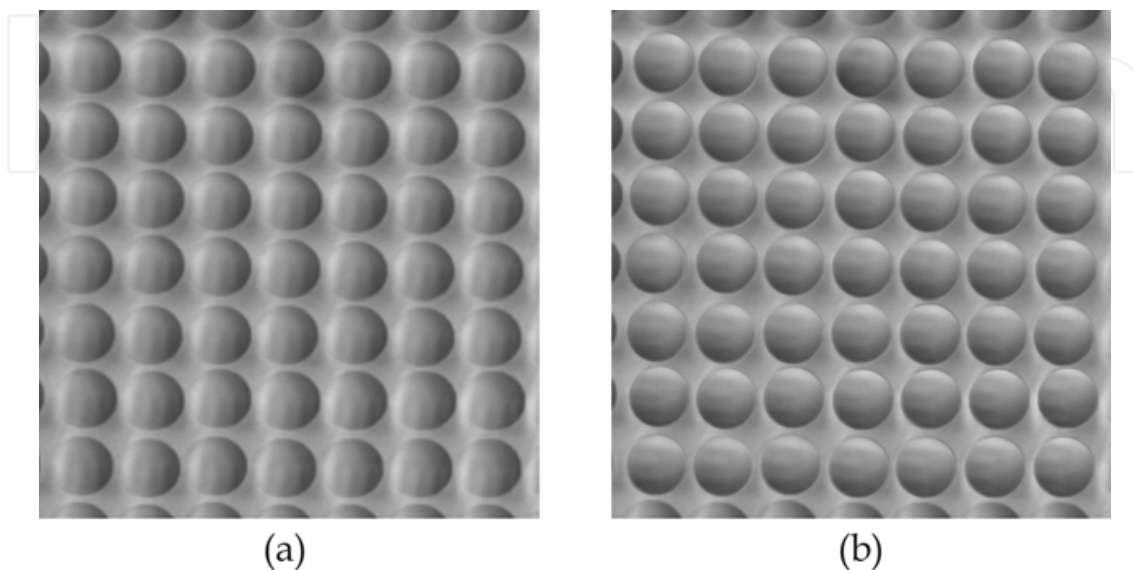

Fig. 13. Image registered on CCD camera for horizontal a) and vertical b) location of the linear filter

In the case of the reconstruction carried out with the use of the Fourier modal method, the results obtained (Fig.14) show the lens whose shape is different from the remaining ones (the central column, bottom row). The reconstruction error E of the lens shape against average for the remaining ones is above 12%. The differences in the shape of the remaining lenses fall within 2%, similarly to the differences in the maximum height of the individual lenses, while the error between the reconstructed shape of the lenses and the theoretical shape of the lenses in the array is within 3%. Such results can be obtained for the 75% of the central surface of the lenses, but on the edges the errors reach 10%. The main difference between the computer simulation and the experimental realization can be noticed in the area between the lenses, which originally is flat. The differences result from the light reflections on the elements of the experimental optical setup, adjustment errors and the non-homogeneity of the amplitude filter used.

In the case of the reconstruction carried out with the use of the Zernike polynomials expansion method, the analysis consisted in the automatic location of the centers of all the lenses, choosing the image of the single lens and applying Zernike expansion method. The operation was carried out for each individual lens. The exemplary results are presented in Fig.15. They show that for the theoretically identical lenses the results obtained are very similar. The maximal difference in the reconstruction between the presented lenses calculated on the basis of Eq.28 is less than 0.5%.

In the next experiment a matrix of 15x5 microlenses was examined. They were all 125 μm in diameter and their shape had been earlier examined with the Wyko profilometer and with the use of Twyman-Green interferometer. The comparison of the results obtained for the

linear filter with 36 Zernike expansion coefficients with the results from interferometry is presented in Fig.16. The horizontal and the vertical cross-sections are very similar, which proves the efficiency of the method used. However, the reconstruction of the full shape of the lenses with the use of the amplitude filter differs from the interferometric results. The differences may result from the errors in adjusting the setup or the tiny scratches on the surface of the test plate around the microlens arrays.
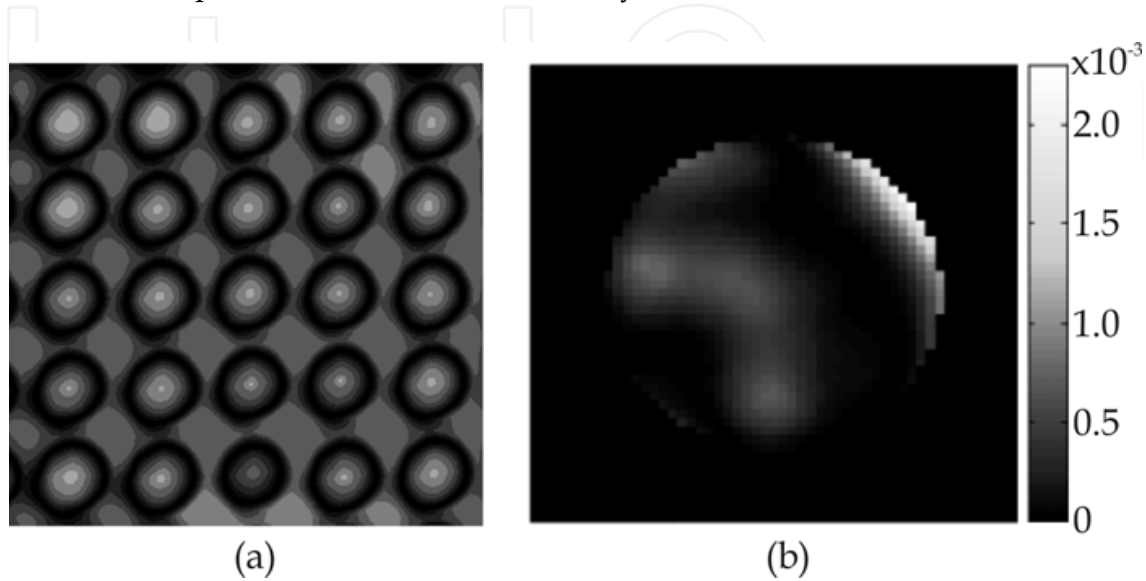
Fig. 14. Fourier-based model reconstruction of the microlenses array a), error E as compared with the ideal lens b) (the lens in the upper left corner)
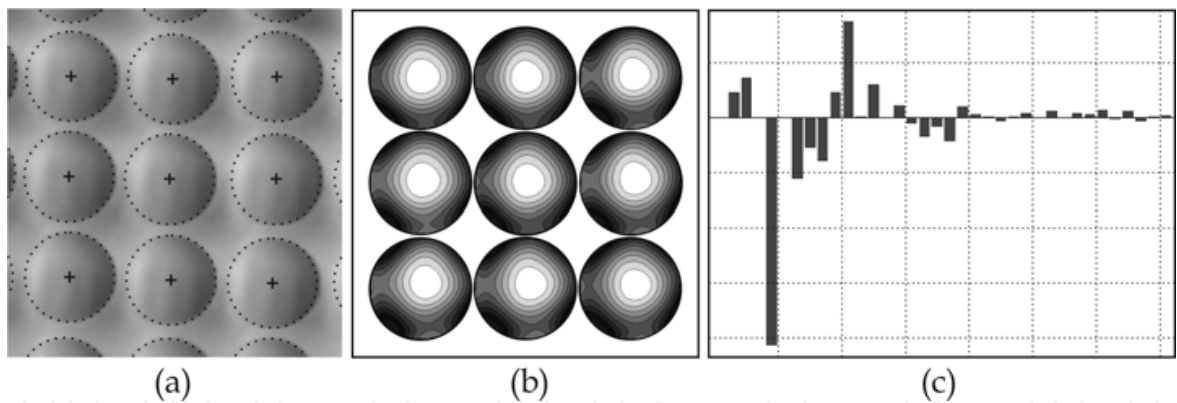
Fig. 15. Zernike reconstruction of the shape of the microlens arrays. The automatically located centers and areas of the individual lenses a), an example of Zernike reconstruction of nine microlenses b) exemplary Zernike expansion coefficients c)

6. Conclusion

The chapter has presented various methods for measuring phase objects and its potential uses. Then it has focused on the use of the amplitude real filter for quality control of microlenses. It presented computer simulations and an experimental realization of an optical setup for automatic quality control of microlens arrays. It has shown that with the use of the simple 4f correlator setup and a single measurement (in the case of two parallel

paths with two perpendicular amplitude filters), as well as a non-complicated computer analysis it is possible to obtain results very close to much more complex, time-consuming and expensive methods. The methods of analysis described here give results slightly less precise than interferometry, especially with the use of the Fourier modal method. On the other hand, they are effective enough for most of the commercial applications in which quality assessment is important.

The main disadvantage of the proposed solution is the necessity to precisely adjust the setup. Also the dependency of the optimal filter width on the parameters of the object examined requires checking several variants of the filters to be used. However, the main advantage of the method, apart from its simplicity, is the possibility of using the whole resolution of the camera, and not its fraction as in the case of the Shack-Hartman method. Using the Zernike polynomials method make the results resistant to the noises present in all optical setups. Moreover, for the Fourier modal method the fact that both the measurement and the analysis are carried out simultaneously for all the objects makes the method much more effective than the ones used so far when fabricating large numbers of microoptical elements.
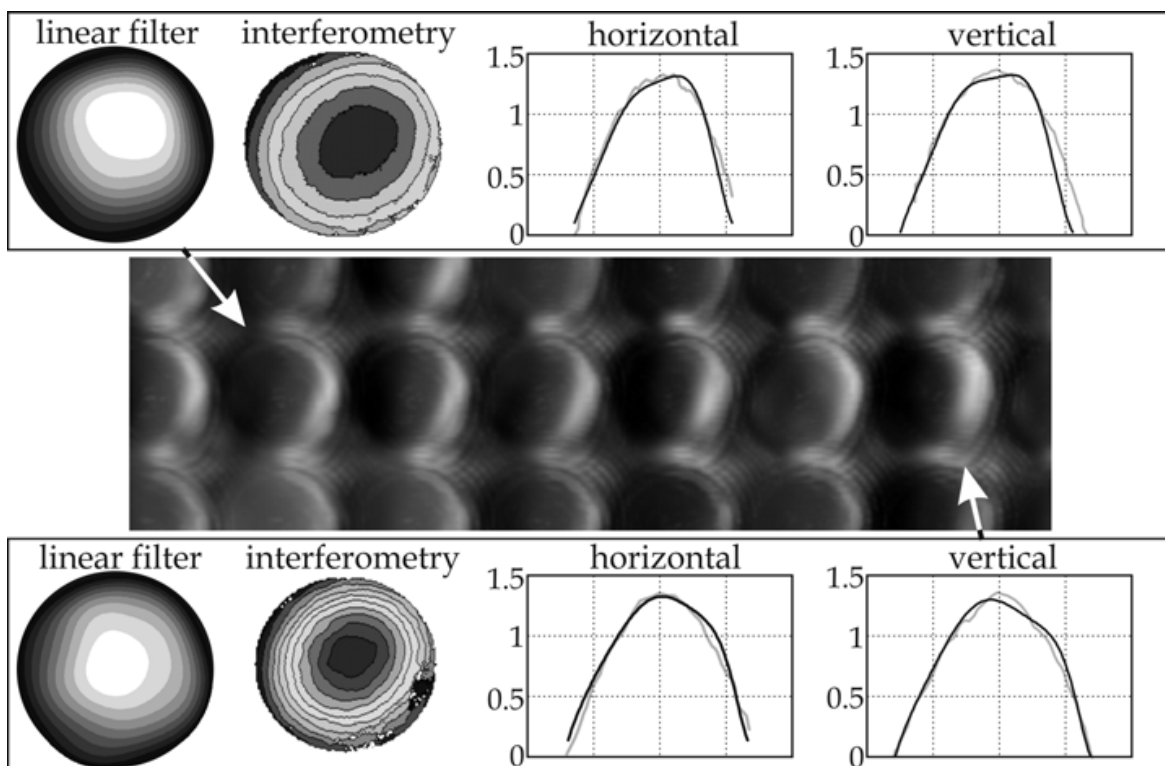

Fig. 16. Zernike reconstruction of the shape of the microlenses (all dimensions given in μm)

7. References

Guang-Ming Dai (2008). *Wavefront Optics for Vision Correction*, SPIE Press Book, ISBN 978-0-8194-6966-3, USA.

Kasztelanic, R. & Sagan, A. (2009). Semiderivative real filter for microoptical elements quality control, *Optical Review*, Vol. 16, No. 3, pp. 252–256, ISSN 1340-6000, Japan.

Settles, G. (2001). *Schlieren and Shadowgraph Techniques*, Springer-Verlag, ISBN 3-540-66155-7, Berlin, Germany.

Wyant, J. & Creath, K. (1992). *Basic wavefront aberration theory for optical metrology*, Applied Optics and Optics Engeenering, Vol. XI. Academic Press, ISBN 0-12-408611-X, New York, USA.

Applications and Experiences of Quality Control

Edited by Prof. Ognyan Ivanov

The rich palette of topics set out in this book provides a sufficiently broad overview of the developments in the field of quality control. By providing detailed information on various aspects of quality control, this book can serve as a basis for starting interdisciplinary cooperation, which has increasingly become an integral part of scientific and applied research.

How to reference

In order to correctly reference this scholarly work, feel free to copy and paste the following:

Rafał Kasztelanic (2011). Quality Control of the Microlenses Array, Applications and Experiences of Quality Control, Prof. Ognyan Ivanov (Ed.), ISBN: 978-953-307-236-4, InTech, Available from: http://www.intechopen.com/books/applications-and-experiences-of-quality-control/quality-control-of-the-microlenses-array

INTECH
open science | open minds